CHAPTER IV
ACTIVITY STUDY OF CARBON XEROGEL DERIVED FROM POLYBENZOXAZINE AS A CATALYST SUPPORT

4.1 Abstract

Recently, a novel nanoporous carbon derived from polybenzoxazine through a sol-gel process has been prepared as a catalyst support. In this work, the activity study of polybenzoxazine derived nanoporous carbon in biodiesel upgrading and photoeletrocatalytic of 4-nitrophenol has also been investigated. Biodiesel has been prepared through partial-hydrogenation of free fatty acid methyl ester (FAMEs) by using $Pd(NO_3)_2.2H_2O$ as a catalyst. The effects of microstructure of carbon xerogel including micro- and meso- porous will be compared with a commercially activated carbon. It can be concluded that the Pd/carbon xerogel used less energy and amount of catalyst for biodiesel upgrading. In case of 4-nitrophenol degradation study, porous TiO_2 was prepared by using carbon xerogel as a template. The photocatalytic degradation by using the resulting porous TiO_2 was compared with the degradation obtained from using TiO_2 loaded on carbon xerogel. It can be concluded that TiO_2 loaded on carbon showed better degradation performance than that of porous TiO_2 since carbon can help adsorp 4-nitrophenol.

Keywords: Carbon Xerogel; Polybenzoxazine; Catalyst support

4.2 Introduction

Carbon-supported catalysts are generally used in chemical industry. The most widely used support is activated carbon, although carbon black or graphite is sometimes considered. Comparing with other types of supports, such as alumina and silica, zeolites; carbon materials have many advantages: (i) they are stable in acid or basic media; (ii) they are resistant to high temperature; and (iii) the metal when used as a catalyst can be recovered easily after burning the support. For some types of carbons, their porous texture can easily be tailored, yielding high surface-area supports where the active phase can be well dispersed with the required pore-size distribution to facilitate the diffusion of reactants and products to, and from, the active phase [1]. Since they are also relative chemically inert, thus, prevent harmful metal-support interactions. Carbons have been utilized as a support for a number of active phases, including noble metals [2], base metal [3], and also metal compounds, such as sulfides and oxides [4].

Carbon aerogels are a novel porous carbon material that has received considerable attention over the past decade [5–9]. These materials can be obtained from the carbonization of organic aerogels prepared from the sol–gel polycondensation of certain organic monomers, such as resorcinol and formaldehyde, following Pekala's method [5, 6]. These carbon aerogels can be obtained in the forms of beads, powders or thin films. Their unique properties, viz. well controlled micro- and mesoporosity, and a large surface area, make them promising materials for application in adsorption and catalysis. Basically, carbon aerogels are a network structure of interconnected nanosized primary particles. In regard of their porous structure, micropores are related to the intra- particle structure whereas mesopores and macropores are produced by the inter-particle structure [10]. The porous structure of carbon aerogel is obtained by solvent removal through supercritical drying process in order to prevent pore collapse. However, this method is impractical for industrial scale production.

Polybenzoxazine (PBZ) provides high thermal stability, low shrinkage upon polymerization, no by-products or volatile generation, excellent dimensional stability, and rich molecular design flexibility. In addition, the supercritical drying process is not necessary due to high crooslink density of polybenzoxazine[11-13].

Porous cabon obtained via ambient drying method is called carbon xerogel. Polybenzoxazine is a great candidate as a polymer precursor to produce carbon xerogel to be used as a material support.

In this study, carbon xerogel derived from polybenzoxazines were developed as a catalyst support. Its performance as a catalyst support for biodiesel upgrading through partial hydrogenation process was compared with the results in which activated carbon was used as a support. The photocatalytic degradation of 4-nitrophenol by using TiO_2 as a catalyst on carbon xerogel was also investigated in comparison with the synthesized porous TiO_2 in which carbon xerogel was used as a template.

4.3 Experimental

4.3.1 Materials

Main-chain type benzoxazine polymer (MCBP) with benzoxazine group as part of the chemical repeat unit was used as a precursor for carbon xerogel. All chemicals were used without further purification. The MCBP was synthesized from bisphenol-A (BA, 97% Aldrich), triethylenetetramine (TETA, FACAI Group Limited, Thailand) and formaldehyde (37% w/w, Merck Limited, Germany) using dimethylformamide (DMF) as a solvent. DMF were purchased from Labscan Asia Co., Ltd., Thailand (analytical grade). Titanium tetrabutoxide (TBOT, Aldrich 97%), 4-nitrophenol, H_2O_2 analytical reagent (30%, Ajax Finechem), Ethyl alcohol, Palladium(II)nitate anhydrous(Aldrich 60%), Biodiesel from Weerasuwan Co., Ltd., Commercial activated carbon (Fluka)

4.3.2 Measurements

The FT-IR spectra of polybenzoxazine precursor and carbon aerogel were obtained on a Nicolet Nexus 670 FT-IR spectrometer. KBr pellet technique was applied in the preparation of powder samples. X-ray diffractometer (Bruker AXS, Germany Model D8 Advance) with CuK_α radiation, a generator voltage of 40 kV, and current of 30 mA. Scanning electron microscope (SEM, JEOL/JSM model 5200) was used to observe the surface morphology of carbon xerogel. Surface areas were calculated using the BET equation. The pore size distributions were constructed

based on Barrett, Joyner and Halenda (BJH) method using the desorption branch of the nitrogen isotherm, measurement Microporous properties were calculated from t-plot method [39], mesoporous properties were analyzed by BJH method [40-41], and specific surface area was determined by BET theory.. UV–VIS spectrophotometer (Shimadzu UV-2550) was used to follow the adsorption of 4-nitrophenol.

4.3.3 Methodology

4.3.3.1. *Synthesis of polybenzoxazine-based carbon xerogels*

4.3.3.1.1 Preparation of BA-teta derived Carbon xerogel

Synthesis of Bisphenol-A and TETA derived benzoxazine precursor(BA-teta) using bisphenol A, formaldehyde and TETA with a mole ratio 1:4:1, as shown in Figure 4.1. Firstly, bisphenol A (4.52 g) was dissolved in dioxane (20 ml) in glass bottle and stirred until the clear solution was obtained. Formaldehyde solution (6.48 g) was then added into the bisphenol A solution. The temperature was kept under 10°C using an ice bath. Diamine (TETA) was then added drop wise into the mixture being continuously stirred for approximately 1 hr until transparent yellow viscous liquid was obtained. The benzoxazine precursor was heated in oil bath at 80°C for 24 hr in a closed system. The partially cured benzoxazine hydrogels were then obtained. After that, solvent removal by ambient pressure drying was conducted for 1 day. The obtained organic xerogel with high porosity [34] were then fully cured by step curing in an oven at 140°, 160°, and 180°C for 2 hr at each temperature and 200°C for 3 hr, respectively.

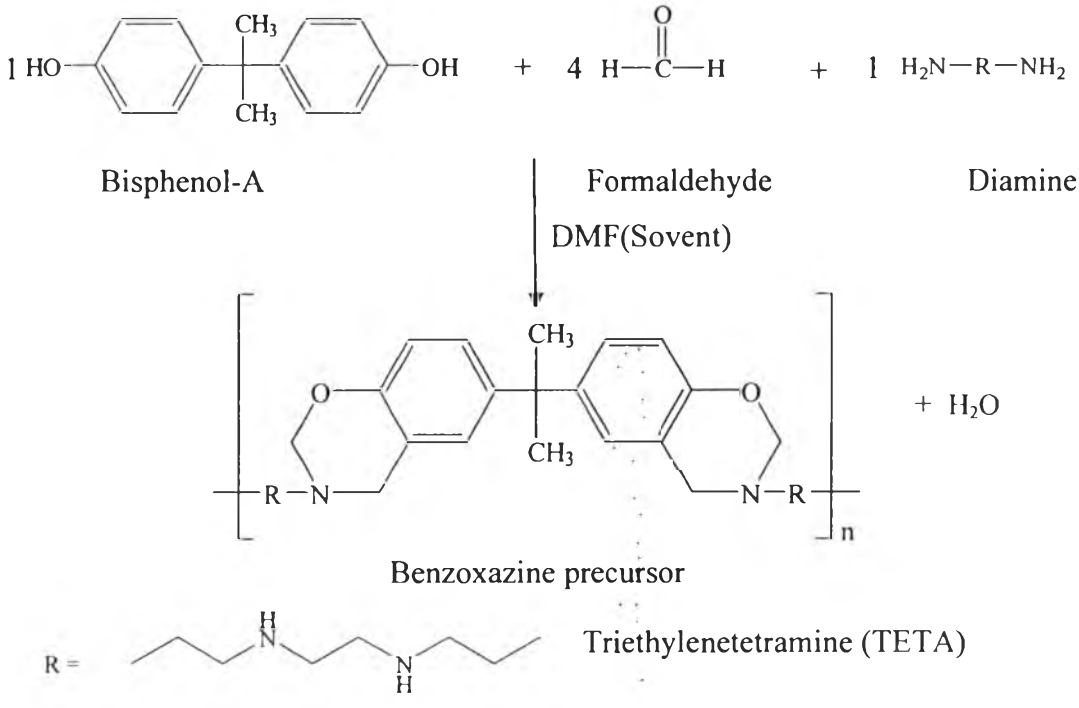

Figure 4.1 Preparation of benzoxazine precursor.

4.3.3.1.2 Pyrolysis process

Pyrolysis was performed at 800°C under nitrogen flow at 500 cm^3/min, using the following temperature program: (i) ramp at 3.7°Cmin^{-1} to 250°C; (ii) ramp at 1.17°Cmin^{-1} to 600°C; (iii) ramp at 3.3°Cmin^{-1} to 800°C and hold for 120 min before slowly cooling to room temperature. After that it will be activated at 900°C in Air for 30 min.

4.3.3.2 *Catalyst Preparation for activity measurement*

4.3.3.2.1 Biodiesel upgrading

Partial hydrogenation experiment of polyunsaturated FAMEs(Free fatty acid methyl ester) will be carried out in a 300 ml stainless steel batch reactor at temperature 120°C and pressure 4 bar. Stirring speed will be maintained at 500 rpm to prevent external mass transfer limitation. The flow rate of hydrogen gas was 50 ml/min. Finally, the liquid products will be collected and analyzed by Hewlett Packard gas chromatography 5890 Series II equipped with a

FID detector. The schematic of the partial hydrogenation experiment is shown in Figure 4.2

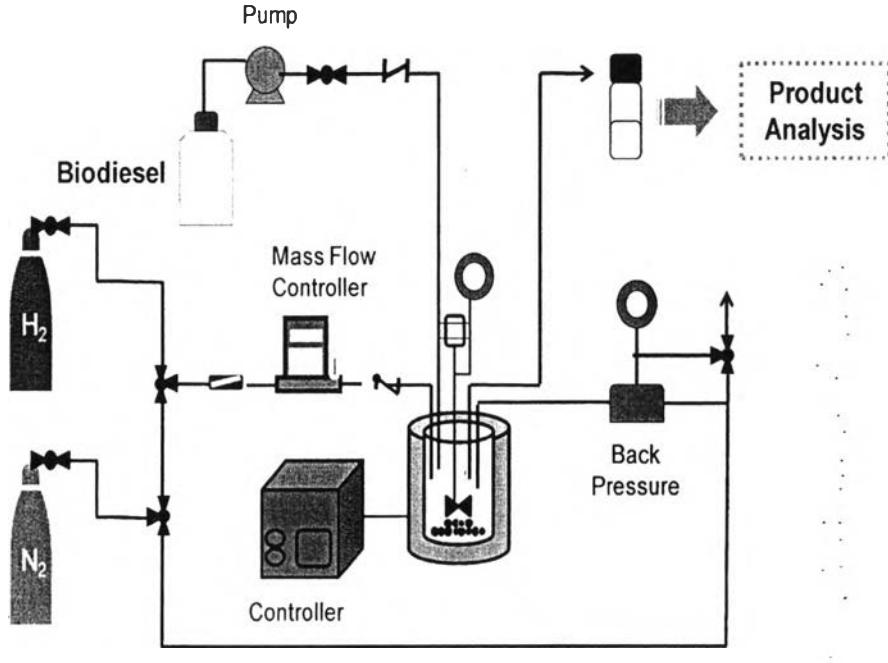

Figure 4.2 Schematic of the partial hydrogenation reaction

Pd (2 wt%) was loaded on the supports(carbon xerogel and activated carbon) by incipient wetness impregnation, wherein a calculated amount of palladium(IV)nitrate dissolved in a minimum amount of water was added dropwise before mixing with the supports. The Pd-loaded supports were then dried overnight before calcining at 500°C for 2 hr to remove the organic moieties.

4.3.3.2.2 Photocatalytic degradation of 4-nitrophenol

In order to study a photocatalytic activity of assynthesized porous titania compared with titania loaded on carbon xerogel, a photocatalytic reactor was used. The batch reactor itself consist of 500 mL glass container with 2 jacks for inline and outline water cooling. 100W Hg Philip UV Lamp was used as a light source. A magnetic stirrer and a cooler was used to keep the reactor at room temperature (Figure 4.3). The concentration of 4-NP used was 10 ppm and the solution was continuously, magnetically stirred. The concentration of a catalyst was fixed at 0.8 g./litre. Ten millimoles per litre of H_2O_2 was then dropped into the

mixture. Sampling of 10 mL of solution was done every 30 minutes untill the illuminating time reach 4 hours to determine the concentration of 4-NP using a Shimadzu UV-240 spectrophotometer.

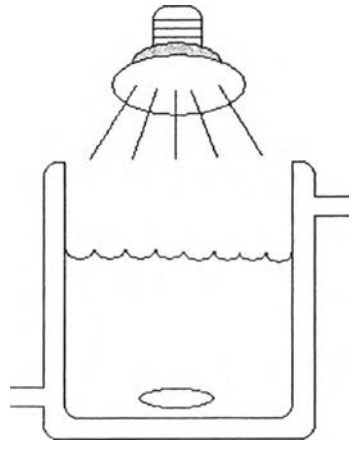

Figure 4.3 the illustration of as studied photocatalst system

The concentration of 4-nitrophenol was resolved with UV-Visible Spectrometer by calibration curve of 4-nitrophenol solution (5, 10, 20, 30 and 40 ppm).

Preparation of porous titania using carbon xerogel as a support. Porous titania was prepared by dissolving titanium tetrabutoxide in ethanol to obtain a concentration of 0.25 M. Then 0.2 g of carbon xerogel was dispersed in 60 ml of TBOT solution by ultrasonic agitation and vacuum for 30 min, respectively. After that, the ample was being placed in air at room temperature for a day and at 80°C for 24 hr to complete the praparation process. TiO_2/carbon xerogel were then pyrolyzed in N_2 at 500°C for 4 h., and calcined in air at 500°C for 24 h, resulting in porous titania.

4.4 Results and Discussion

4.4.1 Characterization of BA-teta derived Polybenzoxazine and Carbon Xerogel

Polybenzoxazine precursor was derived from the reaction of diamine, bisphenol-A and formaldehyde at the molar ratio of 1:1:4 via quasi-solventless approach. Dimethylformamide (DMF) was added with all reactants in order to facilitate the mixing of reactants during the synthesis.

4.4.1.1 Proton Nuclear Magnetic Resonance (^{1}H-NMR)

The chemical structure identification of benzoxazine precursor was carried out using ^{1}H-NMR, as shown in Figure 4.4. The characteristic peaks assigned to the methylene protons of (O–CH_2–N) and (Ar–CH_2–N) of oxazine ring were observed at around 4.82 and 3.94 ppm, respectively. The methyl protons of bisphenol-A were observed at 1.55 ppm. The protons of aliphatic diamine (TETA) show the peaks around 2.86 ppm.

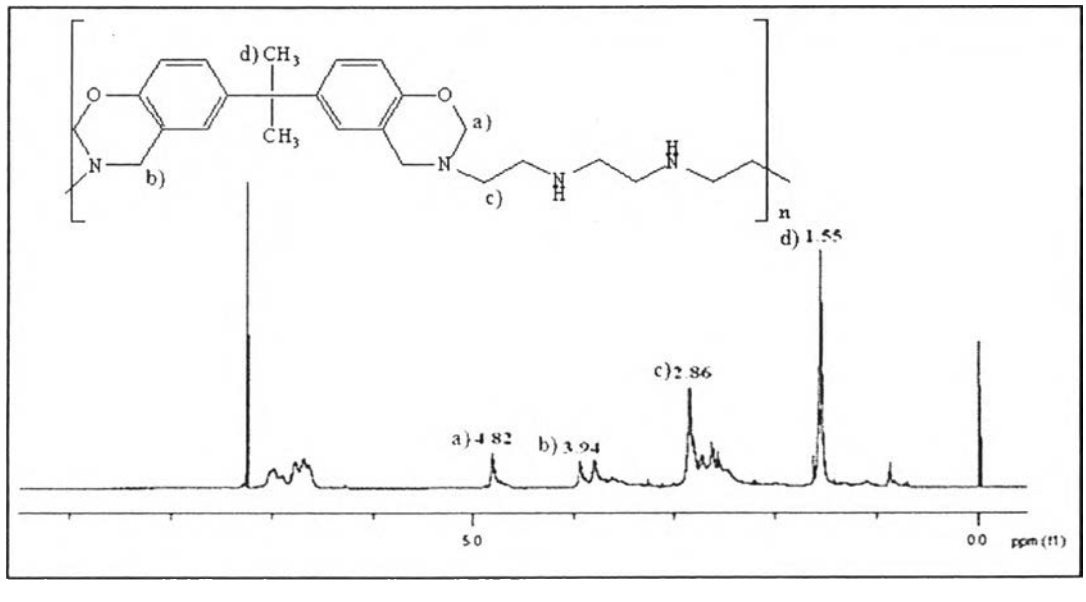

Figure 4.4 ^{1}H-NMR spectrum of benzoxazine precursor.

4.4.1.2 Fourier Transform Infrared Spectroscopy (FT-IR)

The FT-IR spectrum in Figure 4.5a shows the characteristic absorption bands of partially-cured benzoxazine at 1260–1262 cm^{-1} (asymmetric stretching of C-O-C of oxazine), 1180–1187 cm^{-1} (asymmetric stretching of C-N-C), 920–950 cm^{-1} and 1491–1500 cm^{-1} (tri-substituted benzene ring). The absorption band of N-H stretching from TETA was observed around 3420–3429 cm^{-1}. Comparing with FT-IR spectrum of polybenzoxazine (Figure 4.5b), the characteristic absorption bands of fully-cured polybenzoxazine at 920–950 cm^{-1} disappeared. The structure of the fully-cured polybenzoxazine is depicted in Figure 4.6. The FT-IR results are in agreement with the study of Takeichi *et al* [11], who suggested that the characteristic absorption was transformed when ring-opening polymerization of the benzoxazine took place. After pyrolysis, the FT-IR spectrum (Figure 4.5c) is rather flat due to the loss of all organic moieties.

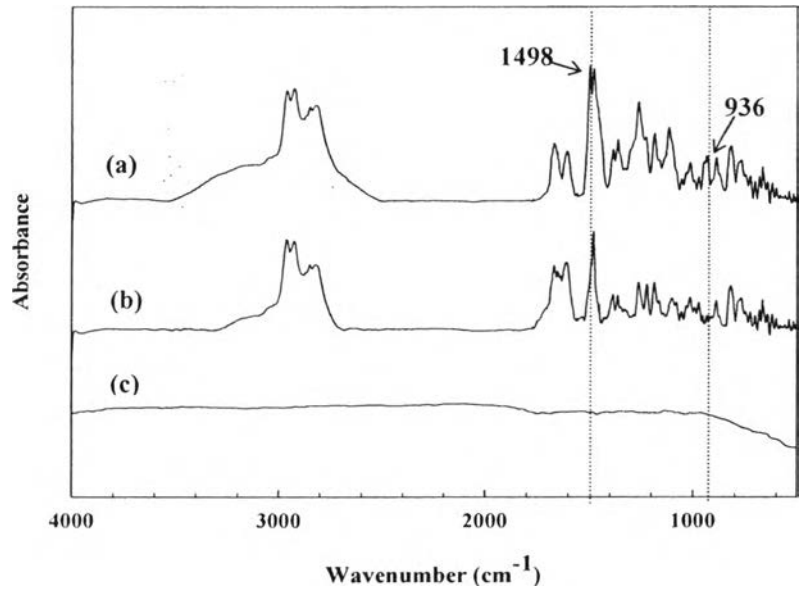

Figure 4.5 FT-IR spectra of benzoxazine precursor at 80°C (partially-cured) (a), polybenzoxazine at 200°C (fully-cured) (b), carbon xerogel at 800°C (c)

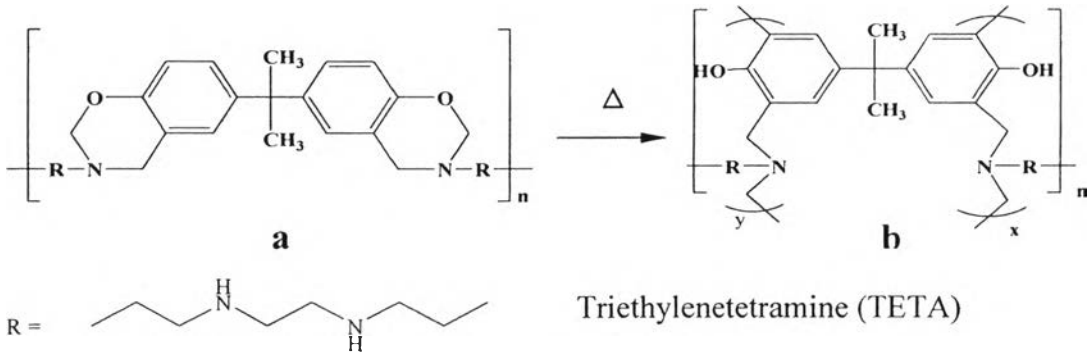

Figure 4.6 The structures of benzoxazine precursor (a), and fully-cured polybenzoxazine (b).

4.4.1.3 Differential Scanning Calorimetry (DSC)

The progress of the ring-opening polymerization from the benzoxazine precusors was monitored by DSC, as shown in Figure 4.7. The DSC thermogram of partially-cured benzoxazine showed the exotherm peak, starting at 180°C with a maximum at 245°C, attributed to the polybenzoxazine ring-opening polymerization. After the polybenzoxazine was fully cured, the exothermal peak disappeared. The same result was also observed by Takeichi *et al.* [13], suggesting that the exotherm peak decreased with the increase of temperature. The exotherm completely disappeared after the end of curing temperature, implying that the ring-opening of oxazine was completed. This evidence can be concluded that the curing reaction of the benzoxazine precursor was practically completed. This DSC result is consistent with the FTIR results.

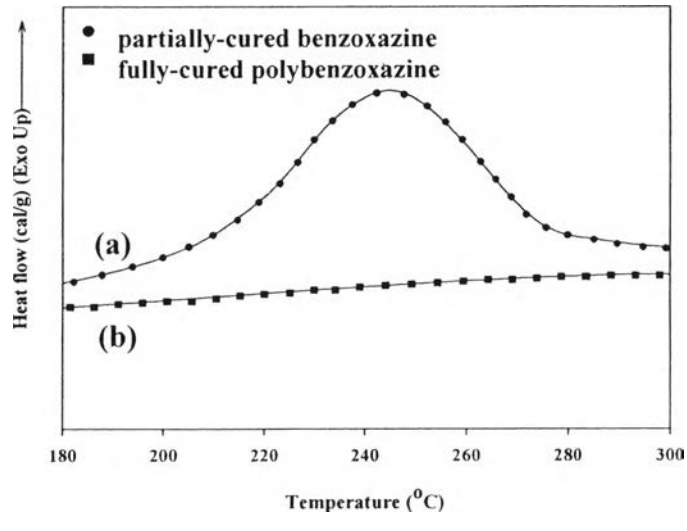

Figure 4.7 DSC thermograms of partially-cured benzoxazine (a) and fully-cured polybenzoxazine (b).

4.4.1.4 Surface and pore characteristics of carbon xerogel (SAA)

The surface and pore characteristics of carbon xerogels and activated carbon xerogel are summarized in Table 4.1. It can be seen that the activated carbon xerogel after pyrolysis in air at 400°C and hold 0.5 hr., the surface area, micropore volume, total pore volume, and average pore size were increased; however, a change in mesopore volume was insignificant.

Table 4.1 Surface characteristics of carbon xerogel and activated carbon xerogel

Parameter	**Carbon Xerogel**	**Carbon Xerogel activation 400** °C
BET surface area (m^2/g)	298	599
Total pore volume (cm^2/g)	0.24	0.39
Average pore size (nm)	2.69	3.14
Micropore volume (cm^3/g)	0.14	0.21
Mesopore volume (cm^3/g)	0.13	0.11
*Mesoporosity (%)	54.1	28.2
*Microporosity (%)	58.3	53.8

*Mesoporosity = (mesopore volume/total pore volume) × 100

*Microporosity = (micropore volume/total pore volume) × 100

4.4.1.5 Morphology of carbon xerogel

The FE-SEM micrographs reveal the pore structure of carbon xerogels prepared from polybenzoxazine via ambient drying. The structure of the carbon xerogel without activation at 400 °C in air composed of interconnected particles in three-dimension network containing continuous macropore (Figure 4.8(a)). In case of activated carbon xerogel, the micrograph also shows similar morphology. However, the pore structure became denser after activation process which might be due to pore collapse.

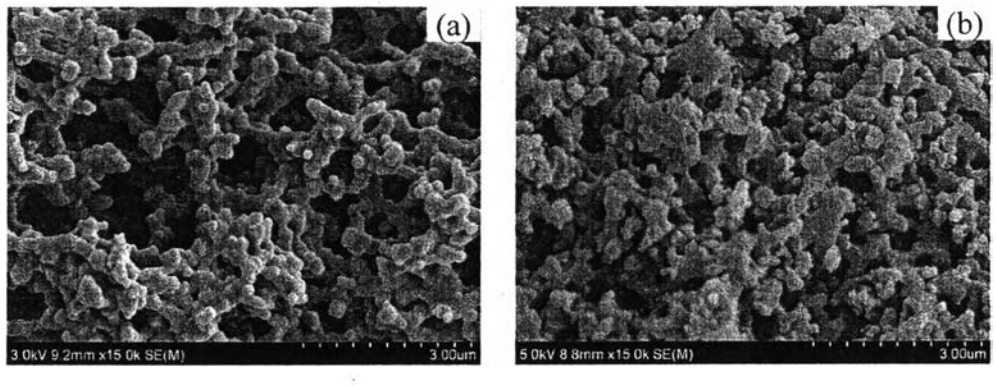

Figure 4.8 FE-SEM micrographs of synthesized carbon xerogels:
(a) carbon xerogel
(b) carbon xerogel activated in air at 400 °C for 0.5 hr.

On the other hand, granule activated carbon is a non-porous material as shown in Figure. 4.9.

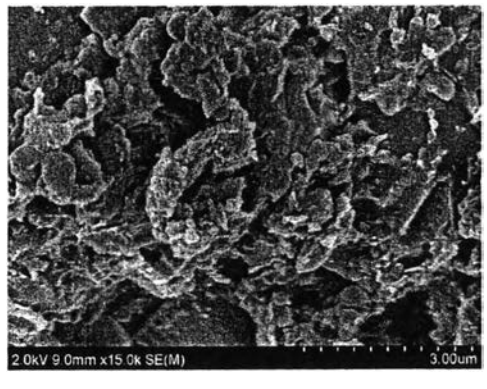

Figure 4.9 FE-SEM micrograph of commercial granule activated carbon.

As shown in Table 4.2, the surface area of activated carbon xerogel was 599 m^2/g, with the total pore volume of 0.39 cm^2/g, and an average pore diameter of 3.15 nm; indicating that activated carbon xerogel was a mesoporous material. Whereas the surface area of non-porous granule activated carbon was 799 m^2/g.

Table 4.2 A comparison of surface characteristics of carbon supports

Parameter	Activated Carbon xerogel	Commercial carbon
BET surface area (m^2/g)	599	799
Total pore volume (cm^2/g)	0.39	N/A
Average pore size (nm)	3.14	N/A
Micropore volume (cm^3/g)	0.21	N/A
Mesopore volume (cm^3/g)	0.11	N/A
*Microporosity (%)	28.2	N/A
*Mesoporosity (%)	53.8	N/A

*Mesoporosity = (mesopore volume/total pore volume) × 100

*Microporosity = (micropore volume/total pore volume) × 100

XRD patterns of fresh and spent 2wt.% Pd supported on carbon aerogel and granule activated carbon were investigated using X-Ray Diffractometer (XRD). Figure 4.10 shows the XRD patterns of (fresh spent Pd supported on) carbon aerogel and granule activated carbon which were prepared by incipient wetness impregnation using $Pd(NO_3)_2.2H_2O$ precursor. The broad signal at about 25° which is assigned to the amorphous carbon was observed in all catalyst (Wu *et al.*, 2009). The main characteristic peak of crystalline Pd plane (111) at 2θ of 40.20 was observed for both Pd/carbon aerogel and Pd/granule activated carbon catalyst after calcination under N_2 at 500°C. The mean particle size of Pd was calculated from the

peak width at half height of the Pd (111) diffraction peak by applying Scherrer's equation are shown in Table 4.3.

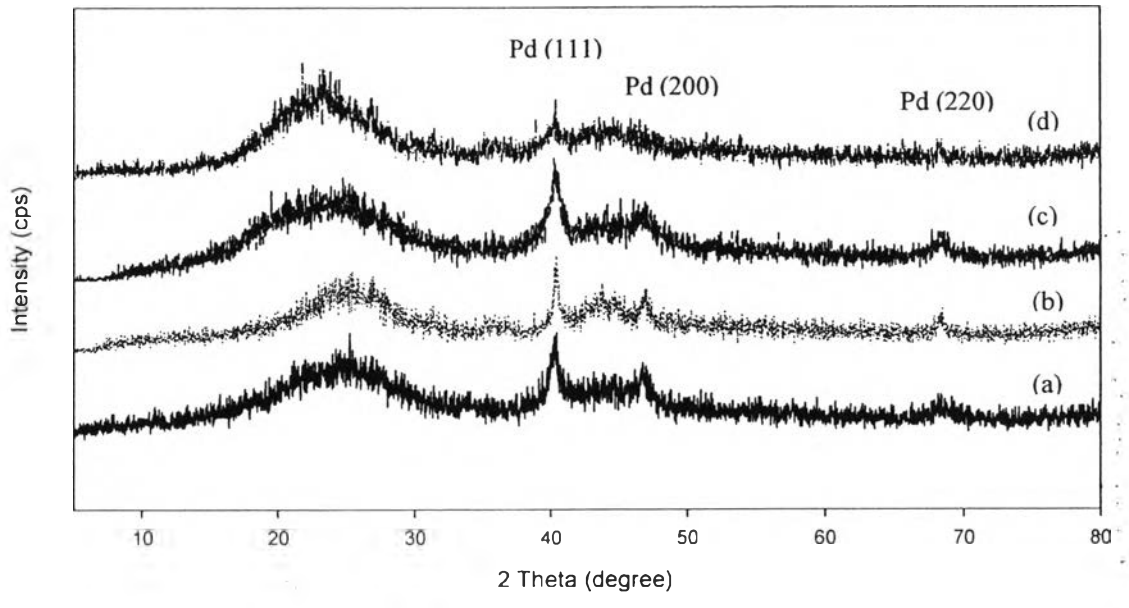

Figure 4.10 XRD patterns of fresh 2wt.% Pd supported on carbon xerogel(a), activated carbon(b), and spent 2wt.% Pd supported on carbon xerogel(c), activated carbon(d)

Table 4.3 The Pd particle size of 2 wt. % Pd/carbon xerogel and granule activated carbon calcined under N_2 at 500°C obtained from XRD technique by applying Scherrer's equation.

Catalyst	Pd (111), nm
Pd/Carbon xerogel	9.97
Pd/Activated carbon	18.5

From Table 4.3, the larger size of Pd/activated carbon could be due to the agglomeration of Pd particles on activated carbon surface. In case of Pd/carbon xerogel, since carbon xerogel is a porous material; therefore, Pd particles can be dispersed in pore structures of carbon xerogel resulting in smaller PD particle size.

4.4.2 Catalytic Activity Testing

4.4.2.1 Biodiesel upgrading by partial-hydrogenation

The effect of types of carbon support was investigated by catalytic activity testing of Pd/carbon xerogel and Pd/ activated carbon in the partial hydrogenation of polyunsaturated FAMEs.

The reaction was operated at a condition of 120°C, 4 bar, 50 ml/min of hydrogen flow rate, 500 rpm of stirring rate, and 1.5 wt.% of catalyst compared to starting oil. The percentages of C18:0, C18:1, C18:2, and other FAMEs (C12:0, C14:0, C16:0, and C22:0) after partial hydrogenation reaction for both types of carbon support are shown in Figure 4.11.

From Figure 4.11a, the Pd/carbon xerogel could rapidly reduce C18:2 and C18:1 from 4.74% to 0.44% and from 29.41% to 7.71%, respectively, after 0.5 h of reaction; while C18:0 sharply increased from 0.41% to 22.82% after 0.5 hour, and continuously increased to almost 32.74% after 4 h of reaction. After only 1.5 hour, C18:2 and C18:1 were completely hydrogenated.

When Pd/activated carbon was used as a support; C18:2 decreased from 4.74% to 1.71% and C18:1 slowly decreases from 29.41% to 24.12%, whereas C18:0 increased from 0.14% to 6.51%, after 0.5 h of reaction as shown in Figure 4.1b. After 2.0 hour of reaction, C18:2 were completely hydrogenated.

Nikolaou *et al.*, (2009) suggested that the higher amounts of saturated FAMEs are less prone to oxidation, but the lower cold flow property would be obtained. If we compare the relative rates of autoxidation of methyl linoleate (C18:2) which is 41 and that of methyl oleate (C18:1) which is 1; it can be deduced that the amount of C18:1 should be kept constant while decreasing the amount of C18:2 in order to improve oxidative stability without affecting the cold flow property.

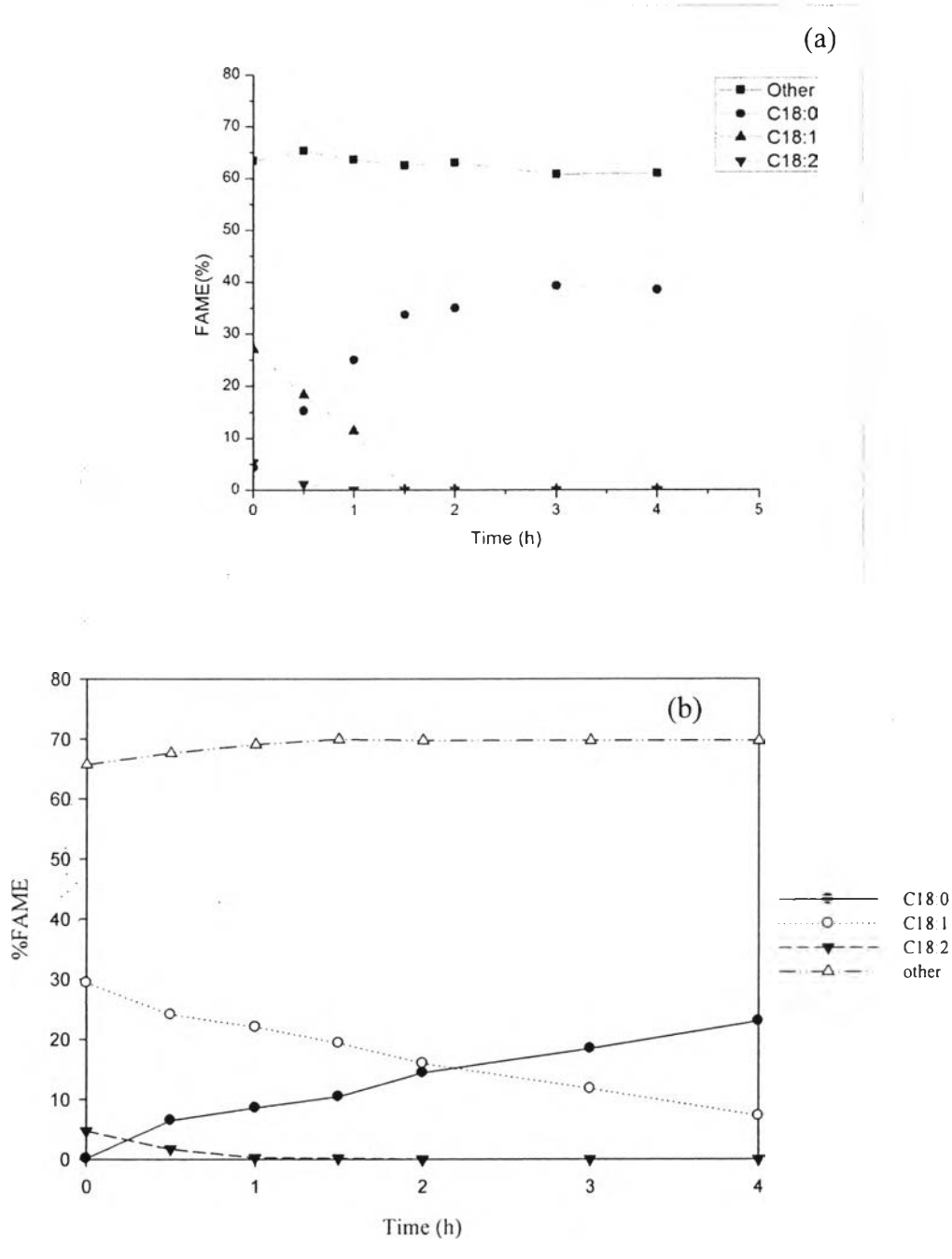

Figure 4.11 Effect of types of carbon support: (a) Pd/carbon aerogel and (b) Pd/commercially activated carbon* on FAME composition of biodiesel after partial hydrogenation reaction (Reaction condition: 120°C , 4 bar, 50 ml/min of H_2 flow rate, 500 rpm of stirring rate, and 1.5 wt.% of catalyst compared with starting oil)

* Data from Mr.Nattapong Thachuangtumle, The Petroleum and Petrochemical College, Chulalongkorn University

Since using carbon xerogel as a support yielded complete hydrogenation, the effect of pressure on partial-hydrogenation process was further investigated. By reducing the pressure, the process will be more economical.

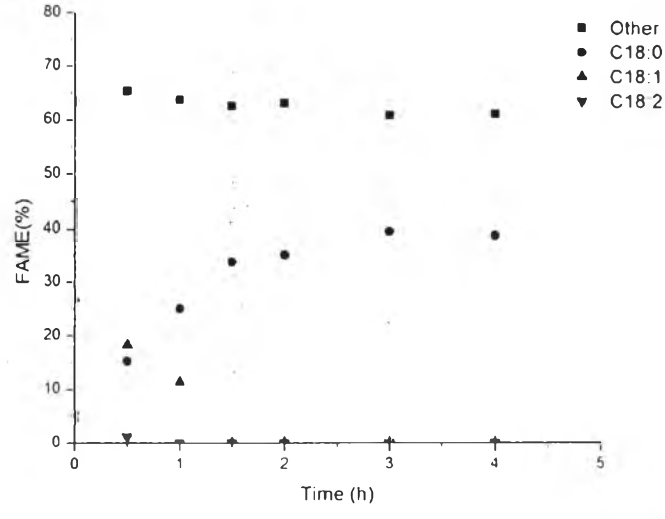

(b)

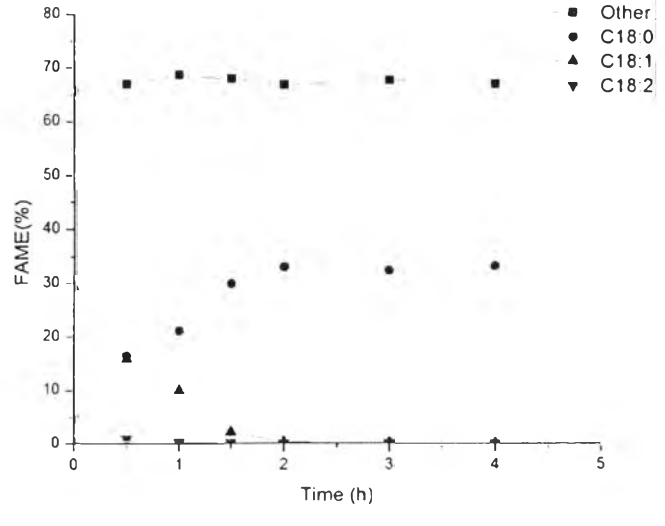

(c)

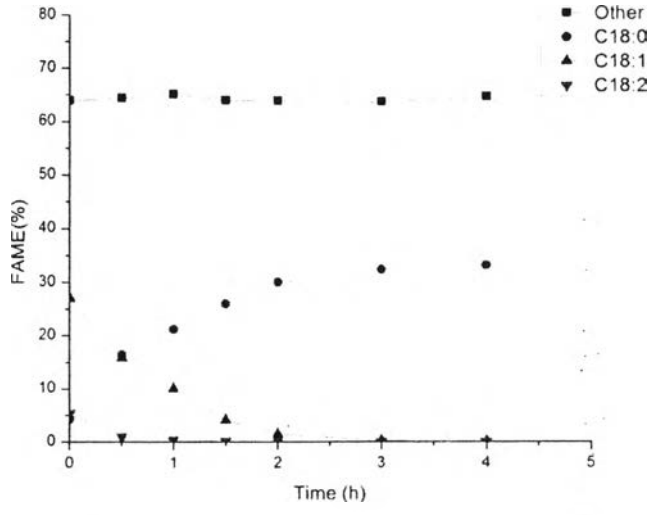

Figure 4.12 Effect of pressure: (a) 4 bar (b) 2 bar and (c) 1 bar
(Reaction condition: 120°C , 50 ml/min of H_2 flow rate, 500 rpm of stirring rate, and 1.5 wt.% of catalyst compared with starting oil)

It was found that the complete hydrogenation process still took place even when the pressure was reduced from 4 bars to 1 bars; therefore, the effect of reaction temperature was further investigated.

(a)

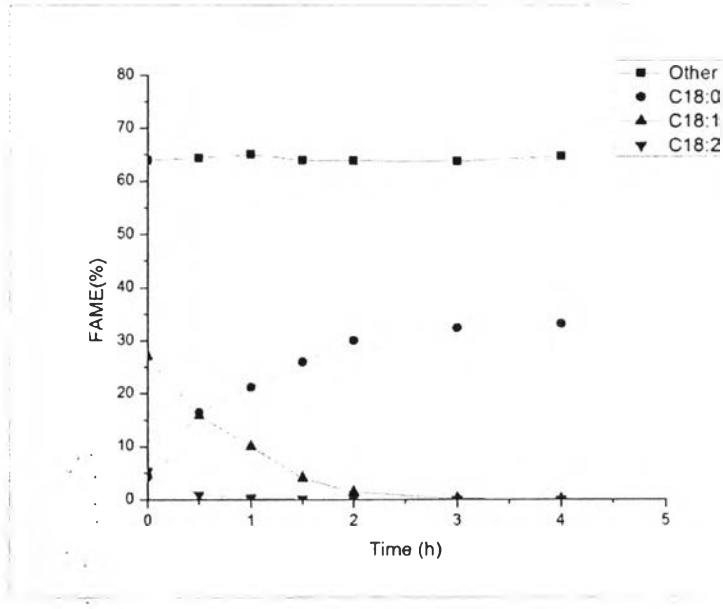
Other
C18:0
C18:1
C18:2
FAME(%)
Time (h)
0
10
20
30
40
50
60
70
80
0
1
2
3
4
5

(b)

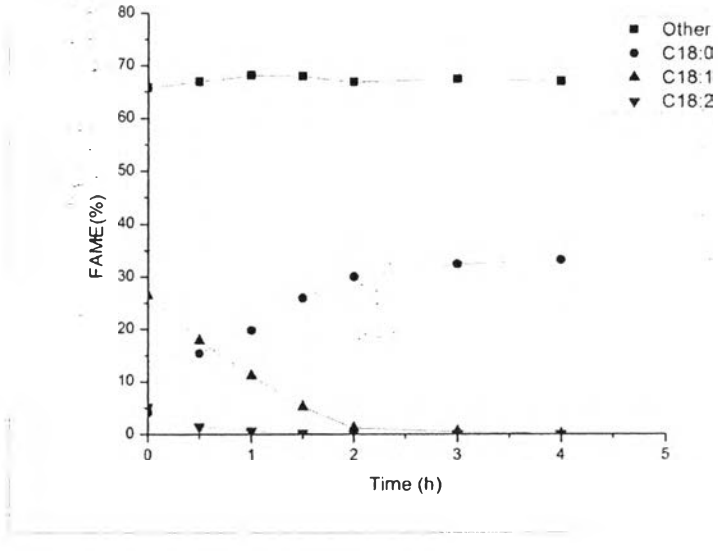
Other
C18:0
C18:1
C18:2
FAME(%)
Time (h)
0
10
20
30
40
50
60
70
80
0
1
2
3
4
5

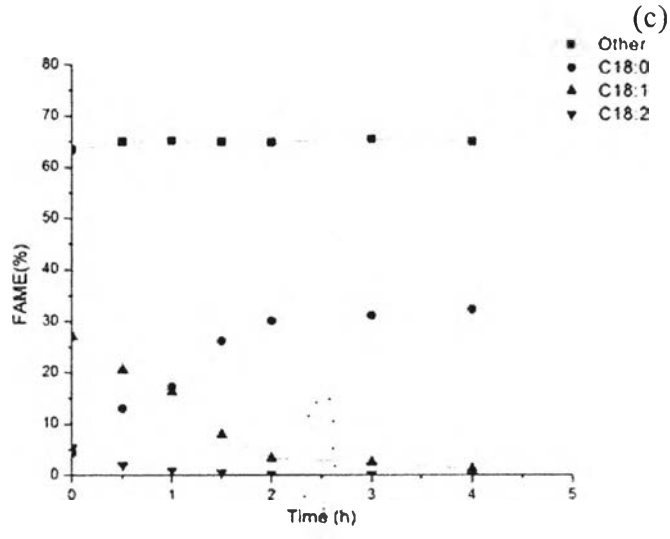

Figure 4.13 Effect of temperature: (a) 120°C (b) 100°C and (c) 80°C
(Reaction condition: 1 bar, 50 ml/min of H_2 flow rate, 500 rpm of stirring rate, and 1.5 wt.% of catalyst compared with starting oil)

By lowering the reaction temperature, the complete hydrogenation still took place when carbon xerogel was used as a support. Therefore, the amount of Pd catalyst was reduced to1.5 wt.% (Figure 4.14). It can be deduced that when carbon xerogel was used as a catalyst support, the energy (pressure, temperature) and amount of catalyst could be reduced for biodiesel upgrading when compared with using granule activated carbon as a support.

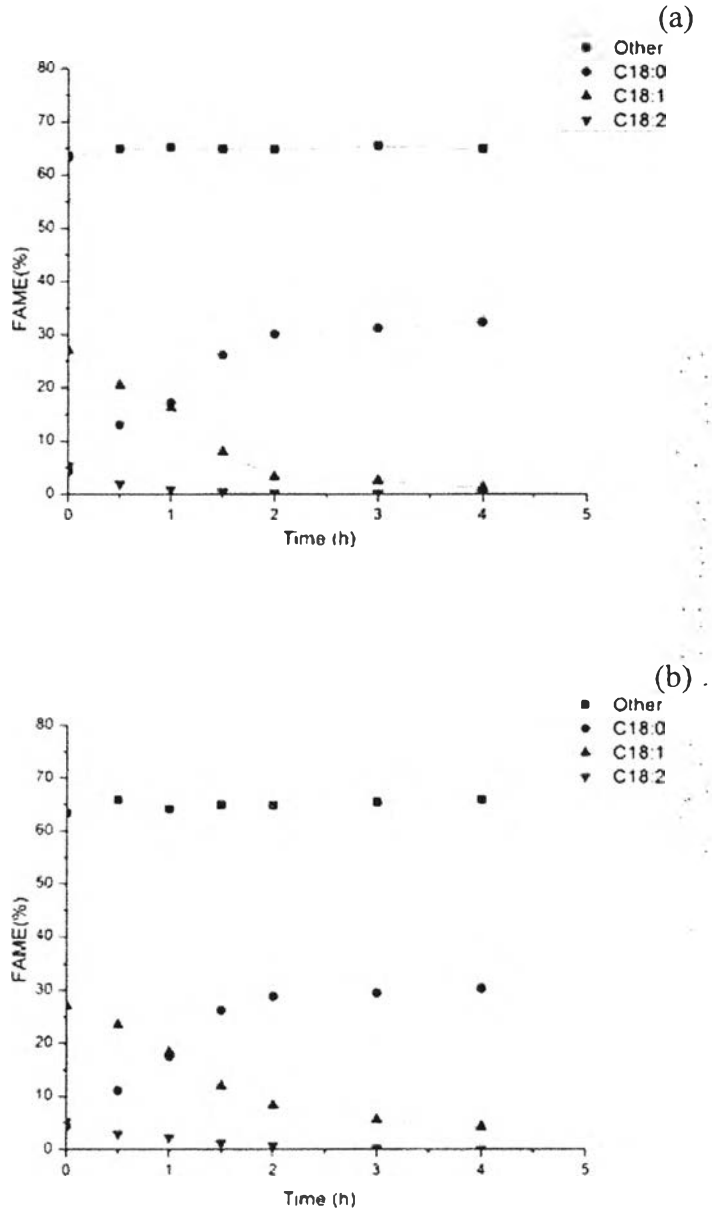

Figure 4.14 Effect of amount of catalyst compared with starting oil: (a) 1.5 wt% and (b) 0.75 wt% (Reaction condition: 80°C, 1 bar, 50 ml/min of H_2 flow rate, and 500 rpm of stirring rate)

Effect of carbon xerogel only was studied by using reaction condition as 120°C, 4 bar, 50 ml/min of H_2 flow rate, and 500 rpm of stirring rate and 1.5 wt.% of catalyst compared with starting oil as shown in Figure 4.15. The results showed that only carbon support which was not adding $Pd(NO_3)_2.2H_2O$ was not active to improve properties of FAMEs.

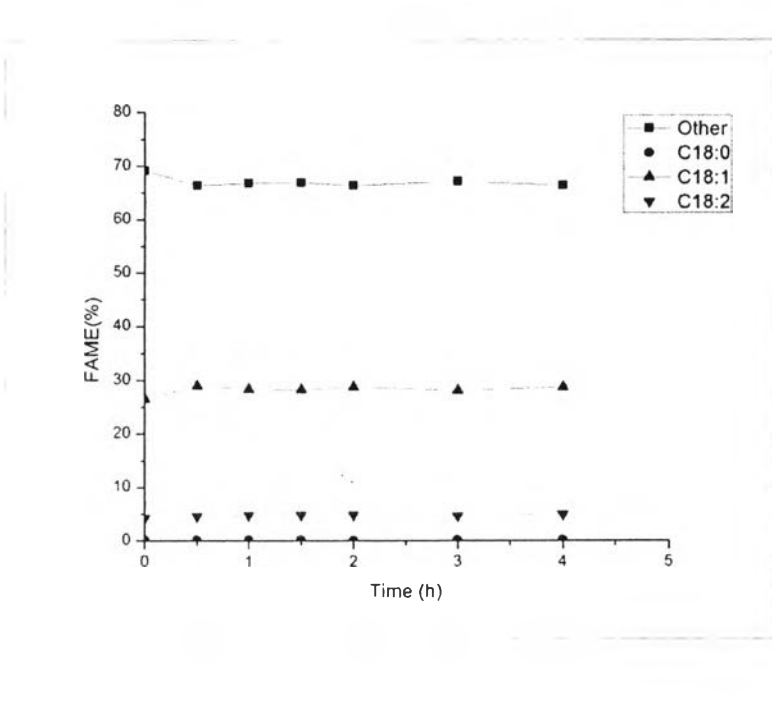

Figure 4.15 Effect of carbon xerogel only (Reaction condition: 120°C, 4 bar, 50 ml/min of H_2 flow rate, and 500 rpm of stirring rate and 1.5 wt.% of catalyst compared with starting oil)

4.4.2.2 Photocatalytic degradation of 4-nitrophenol

In photocatalysis applications, both crystal structures of TiO_2, i.e. anatase and rutile, are commonly used, with anatase showing a greater photocatalytic activity for most reactions[16]. The X-ray diffraction pattern (Figure 4.2) reveals sharp peaks of anatase phase and small amount of rutile was also observed at a reaction time of 30 minutes. The longer reaction time resulted in gradual reduce of anatase and rutile titania phase and developing of new peaks observed at 2θ~10°, 24°, 28° and 48°. The peak at 10° resembled the layered wall structure of titanate.

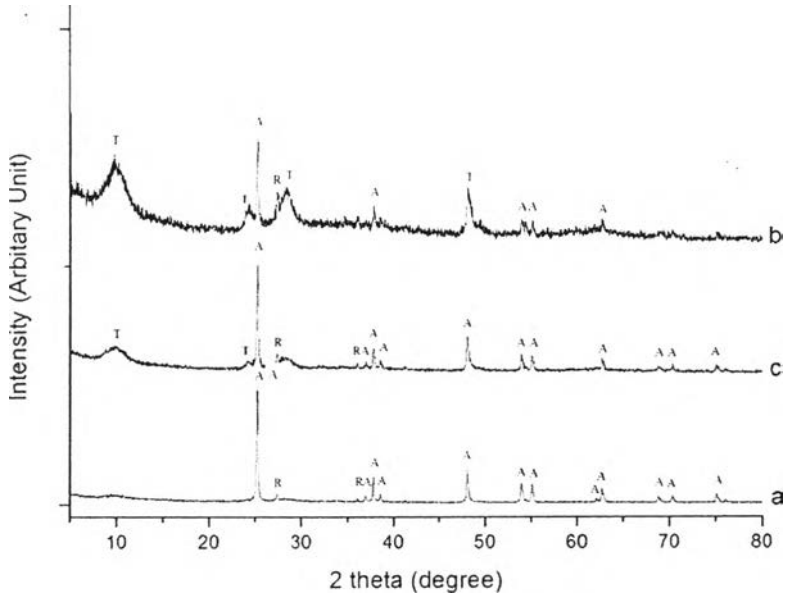

Figure 4.16 X-ray diffraction spectra of titania (a) without using carbon xerogel as a template (b) useing carbon xerogel as a template (c) support on carbon xerogel

From SEM micrographs, the particle size of synthesized TiO_2 without using carbon xerogel as a template (Figure 4.16 (a)) is larger than that of synthesized TiO_2 in which carbon xerogel was used as a template (Figure 4.16 (b)).

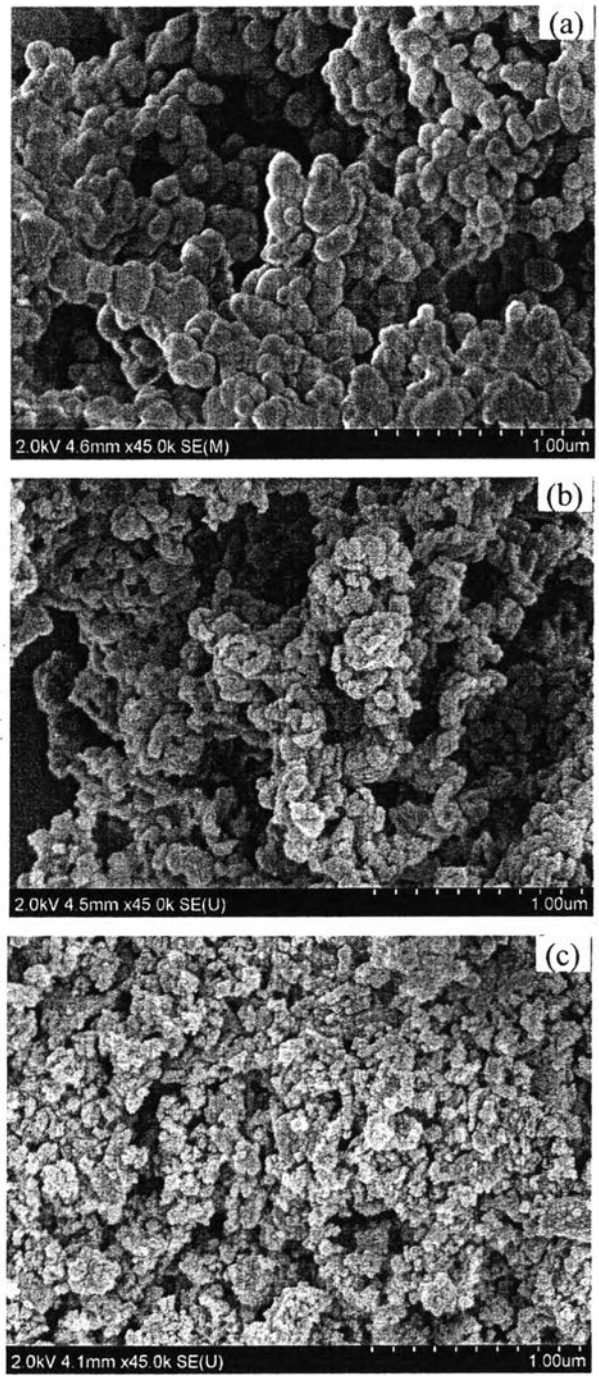

Figure 4.17 FE-SEM micrographs of titania study type (a) Titania synthesized without using carbon xerogel as a template, (b) synthesized Titania using carbon xerogel as a template, (c) Titania on carbon xerogel

The surface characteristics of different types of titania used in the photocatalytic degradation study are summarized in Table 4.4.

Table 4.4 The Surface characteristics of different types of titania used in the photocatalytic degradation study

Type of Titania	Surface area (m^2/g)	Total pore volume (ml/g)	Average pore diameter (nm)
Without using carbon xerogel as a template	19.62	0.1092	0.045
Using carbon xerogel as a template	93.43	0.37	16.14
Using carbon xerogel as a support	478.1	0.5991	2.768

As shown in Figure 4.17, by using carbon xerogel as a template, 4-nitrophenol degraded significantly faster than prestine TiO_2 which might be due to porous TiO2 could adsorb 4-nitrophenol on the surface, increasing the reaction activity. However, the degradation performance was the best when TiO2 was loaded on carbon xerogel support since carbon xerogel was a better adsorbent than porous TiO_2, resulting in further enhanced the reaction activity. However, TiO2 is still necessary for the degradation of 4-nitrophenol since it acts as a catalyst. As shown in Table 4.4, the degradation of 4-nitrophenol was reduced in the beginning of the reaction due to carbon xerogel acted as an adsorbent; however, when TiO_2 was not used as a catalyst, the amount of 4-nitrophenol was maintained at a certain level after the reaction was progressed.

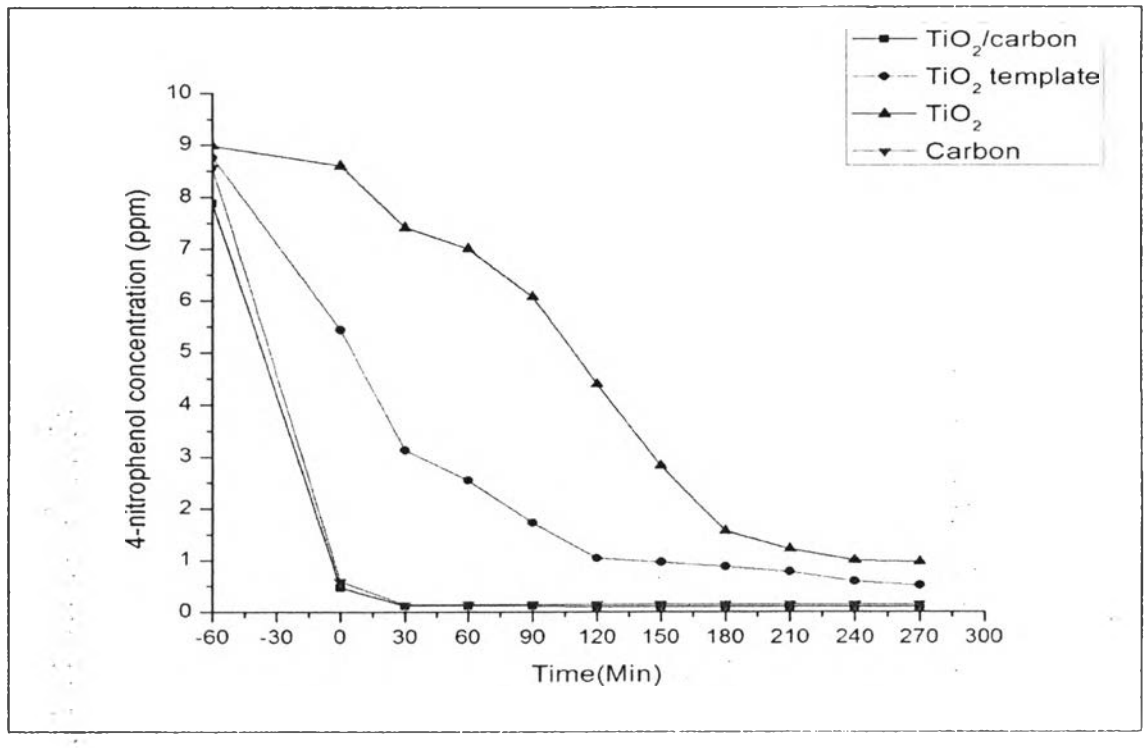

Figure 4.18 The adsorption of 4-NP vs. the reaction time of Titania synthesized by not used carbon xerogel (-▲-), Titania using carbon xerrogel as a template (-●-), Titania loaded on carbon xerogel(-■-), and carbon xerogel only (-▼-)

Table 4.5 The concentration of 4-Nitrophenol (ppm) at a given UV irradiation each time when carbon xerogel was used as a support, compared with a blank (TiO_2 was not loaded on a carbon xerogel support)

Time	TiO2/Carbon xerogel	Carbon xerogel only
-60	7.8827	8.56534
0	0.47252	0.58872
30	0.12561	0.14333
60	0.12674	0.14861
90	0.12138	0.1475
120	0.10109	0.14677
150	0.09573	0.14689
180	0.10404	0.14595
210	0.09932	0.14701
240	0.09897	0.14632
270	0.09725	0.14813

4.5 Conclusions

By using carbon xerogel as a support in biodiesel upgrading, the energy (pressure and temperature) and amount of catalyst can be reduced, when compared with using granule activated carbon. Moreover, carbon xerogel can be used as a TiO_2 support for photocatalytic degradation of 4-nitrophenol. Carbon xerolge also acted as an adsorbent which resulted in an enhancement of photocatalytic degradation when compared with commercial TiO_2 or synthesized porous TiO_2 using carbon xerogel as a template.

4.6 Acknowledgements

The authors wish to thank the National Center of Excellence for Petroleum, Petrochemicals, and Advanced Materials, Chulalongkorn University and the Petroleum and Petrochemical College for the financial support. A great appreciation is also extended to Asst. Prof. Apanee Luengnaruemitchai for her guidance and instrumental facility on biodiesel upgrading.

4.7 References

[1]. RodrõÂguez-Reinoso, F., RodrõÂguez-Ramos, I., Moreno-Castilla, C., Guerrero-Ruiz, A., and LoÂpez-GonzaÂlez, J.D. (1986). Platinum catalysts supported on activated carbons: I. Preparation and characterization. Journal of Catalysis, 99, 171.

[2]. Neri, G., Musolino, M.G., Milone, C., Visco, A.M., and DiMario, A. (1995). Mechanism of 2,4-dinitrotoluene hydrogenation over Pd/C. Journal of Molecular Catalysis A Chemical, 95, 235.

[3]. Bischoff, S., Weight, A., Fujimoto, K., and LuÈcke, B. (1995). The role of promoter metals in the hydrocarbonylation of methanol over active carbon supported cobalt catalysts. Journal of Molecular Catalysis A Chemical, 95, 259.

[4]. Drago, R.S., Jurczyk, K., Singh, D.J., and Young, V. (1995). Low-temperature deep oxidation of hydrocarbons by metal oxides supported on carbonaceous materials. Applied Catalysis B: Environmental, 6, 155.

[5]. Pekala, RW. US patent 4873218. (1989).

[6]. Pekala, RW., Alviso, CT., Kong, FM., and Hulsey, SS. (1992). Aerogels derived from multifunctional organic monomers. Journal of Non-Crystalline Solids, 145, 90–98.

[7]. Maldonado-Ho´dar, FJ., Ferro-Garcı´a, MA., Rivera-Utrilla, J., Moreno-Castilla, C. (1999). Synthesis and textural characterization of organic aerogels, transition-metal-containing organic aerogels and their carbonized derivatives. Carbon, 37, 1199–1205.

[8]. Pierre, AC., and Pakonk, GM. (2002). Chemistry of aerogels and their applications. Chemical Reviews, 102, 4243–4265.

[9]. Al-Muhtaseb, SA., and Ritter, JA. (2003). Preparation and properties of resorcinol–formaldehyde organic and carbon gels. Advanced Materials, 15, 101 –114.

[10]. Yoshizawa, N., Hatori, H., Soneda, Y., Hanzawa, Y., Kaneko, K., and Dresselhaus, MS. (2003). Structure and electrochemical properties of carbon aerogels polymerized in the presence of Cu^{2+}. Journal of Non-Crystalline Solids, 330, 99–105.

[11]. Ishida, H. US Patent 5, 543, 516, assigned to Edison Polymer Innovation Corporation.

[12]. Ishida, H., and Allen, D. (1996). Physical and mechanical characterization of near-zero shrinkage polybenzoxazines. Journal of Polymer Science Part B, 34(6), 1019–1030.

[13]. Agag,T., and Takeichi, T. (2003). Synthesis and characterization of novel benzoxazine monomers containing allyl groups and their high performance thermosets. Macromolecules, 36, 6010-6017.

[14]. Azaïs, P., Duclaux, L., Florian, P., Massiot, D., Lillo-Rodenas, MA., Linares-Solano, A., Peres, JP., Jehoulet, C., and Béguin, F. (2007) Causes of supercapacitors ageing in organic electrolyte. Journal of Power Sources, 171, 1046-1053.

[15]. Takeichi, T., Kano, T., and Agag, T. (2005). Synthesis and thermal cure of high molecular weight polybenzoxazine precursors and the properties of the thermosets. Polymer, 46, 12172–12180.

[16]. Lorjai, P., Chaisuwan T., and Wongkasemjit S., Journal of Sol-gel Science and Technology, submitted.

[17]. Garea, S.A., Iovu, H., Nicolescu, A., and Deleanu, C. (2007). Thermal polymerization of benzoxazine monomers followed by GPC, FTIR and DETA. Polymer Testing, 26, 162–171.

[18]. Kasinee, H., and Ishida, H. (2002). Thermal decomposition processes in aromatic amine-based polybenzoxazines investigated by TGA and GC–MS. Journal of Polymer, 37, 4391-4402.

[19]. Takeichi, T., Kano, T., and Agag, T. (2005). Synthesis and thermal cure of high molecular weight polybenzoxazine precursors and the properties of the thermosets. Polymer, 46, 12172-12180.

[20]. Tamon, H., Ishizaka, H., Mikami, M., and Okazaki, M. (1997) Porous structure of organic and carbon aerogels synthesized by sol-gel polycondensation of resorcinol with formaldehyde. Carbon, 35, 791-796.

[21]. Wang, J., Yang, X., Wu, D., Fu, R., Dresselhaus, M.S., and Dreaaelhaus, G. (2008) The porous structures of activated carbon aerogels and their effects on electrochemical performance. Journal of Power Sources, 185, 589-594.

[22]. Wang, J., Zhang, S.Q., Guo, Y.Z., Shen, J., Attia, S.M., Zhou, B., Zheng, G.Z., andGui, Y.S. (2001) Morphological effects on the electrical and electrochemical properties of carbon aerogels. Journal of The Electrochemical Society, 148, D75-D77.

[23]. Zhang, R., Lu, Y., Zhan, L., Liang, X., Wu, G., and Ling, L. (2002) Monolithic carbon aerogels from sol–gel polymerization of phenolic resoles and methylolated melamine. Carbon, 41, 1645-1687.

[24]. Wen-Cui, L., An-Hui, L, and Shu-Cai, G. (2001). Characterization of the microstructures of organic and carbon aerogels based upon mixed cresol–formaldehyde. Carbon, 39, 1989–1994.

[25]. Yan, J., and Zhang, Q.Y. (1979). Adsorption and Desorption. Beijing Science Press, 96.

[26]. Shen, J., Hou, J., Guo, Y., Xuem, H., Wu, G., and Zhou, B. (2005). Microstructure control of RF and carbon aerogels prepared by sol-gel process. Journal of Sol-Gel Science and Technology, 36, 131–136.

[27]. Guifen, L., Dingcai, W., and Ruowen, F. (2008). Performance of carbon aerogels particle electrodes for the aqueous phase electro-catalytic oxidation of simulated phenol wastewaters. Journal of Hazardous materials, 39, 187-193.